IEPC-95-34

SIMPLIFIED NUMERICAL DESCRIPTION OF SPT OPERATION

DAVID H. MANZELLA*

Abstract

A simplified numerical model of the plasma discharge within the SPT-100 stationary plasma thruster was developed to aid in understanding thruster operation. A one dimensional description was used. Non-axial velocities were neglected except for the azimuthal electron velocity. A nominal operating condition of 4.5 mg/s of xenon anode flow was considered with 4.5 Amperes of discharge current, and a peak radial magnetic field strength of 130 Gauss. For these conditions, the calculated results indicated ionization fractions of 0.99 near the thruster exit with a potential drop across the discharge of approximately 250 Volts. Peak calculated electron temperatures were found to be sensitive to the choice of total ionization cross section for ionization of atomic xenon by electron bombardment and ranged from 51 eV to 60 eV. The calculated ionization fraction, potential drop, and electron number density agree favorably with previous experiments. Calculated electron temperatures are higher than previously measured.

Nomenclature

A	Cross sectional area of discharge chamber
A	Coefficient matrix
a_0	Bohr radius
$\vec{b}$	Column vector of inhomogeneous terms
B_r	Radial magnetic field strength
D_e	Electron diffusion coefficient
E_i	Ionization energy
E_i^H	Ionization energy of hydrogen
$\vec{E}$	Electric field
e	Elementary charge
$f(E)$	Electron energy distribution function
J	Discharge current
J_e	Electron current density
k	Boltzmann's constant
k_i	Volumetric rate of ionization
L	Discharge length (anode to cathode)
m	Mass flow rate
m_a	Atom mass
m_e	Electron mass
m_i	Ion mass
n_a	Atom number density
n_e	Electron number density
n_i	Ion number density
P_e	Electron pressure
$Q(E)$	Collision cross section
q_e	Conductive heat flux due to electrons
T_a	Atom temperature
T_e	Electron temperature
T_i	Ion temperature
$\vec{U}_e$	Electron drift velocity
U_e	Axial electron drift velocity
$U_{e\theta}$	Circumferential electron drift velocity
U_a	Electron drift velocity
U_i	Ion drift velocity
w	Net rate of electron/ion production
z	Spatial coordinate
$\vec{x}$	Column vector of unknowns
ε_i	Ionization energy
μ_e	Electron mobility
$<\sigma>$	Average collision cross section
ν_{ai}	Atom ion momentum transfer collision frequency
ν_{ea}	Electron atom momentum transfer collision frequency
ν_{ei}	Electron ion momentum transfer collision frequency
ϕ	Electric potential

Introduction

During stationary plasma thruster operation a plasma is sustained within an annular discharge chamber by an axial electric field established between an external hollow cathode and an anode located at the rear. Near the anode, electron-ion pairs are formed through collisional ionization via electron bombardment. The interaction between the electrons and the crossed axial electric field and radial magnetic field established by electromagnets redirects the electrons in a azimuthal direction greatly reducing the electron conductivity in the axial direction. The reduced axial electron conductivity permits large electric fields which efficiently accelerate thrust producing ions. A cross sectional schematic of the discharge chamber is shown in Figure 1. The objective of this investigation was to develop a tool capable of examining the details of these processes using the minimum subset of the governing equations required to retain all

* Research Engineer, NYMA, Inc. Engineering Services Division, Brook Park, Ohio U.S.A.

essential physical phenomenon. As a result of this approach, non-axial velocities were neglected except for azimuthal electron velocity. These limitations prevent direct insight into important issues such as thruster lifetime and spacecraft integration associated with non-axial ion velocities but allow numerical solutions of the discharge physics to be obtained using a personal computer in a timely fashion.

Specifically, the model consisted of seven coupled algebraic and differential equations. These included ion continuity, global continuity, current continuity, ion momentum, electron momentum and electron energy. Assumptions included one dimensional flow, quasi-neutrality, no doubly charged ions, constant and equal atom and ion temperatures, and constant atom velocity. Seven unknowns were calculated: electron/ion density, atom density, ion velocity, electron velocity, electron temperature, and potential. Initial conditions included discharge current, mass flow rate, initial ionization fraction and initial electron temperature. The axial distribution of the radial magnetic field was also assumed. This approach differs from that of past investigators. Melikov's[1] one-dimensional model relied on experimentally determined values for the potential and electron temperature distribution. Lentz[2] relied on Bohm diffusion to describe the axial motion of the electrons across the magnetic field lines. More recently, Fife[3] has successfully extended this work to include both axial and radial dimensions.

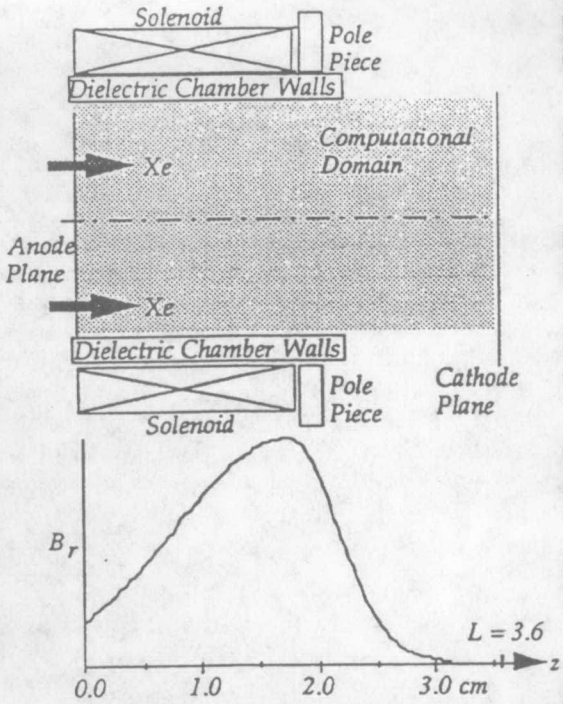

Figure 1: Cross Sectional Schematic of the Annular Section of the SPT Discharge Chamber and Assumed Radial Magnetic Field Distribution.

In this paper, model formulation is presented including additional assumptions and simplifications not previously mentioned. The first-order explicit solution technique is also presented. Calculated results are presented as is the sensitivity of these results to the initial conditions and inputted parameters. Finally, where appropriate, the results are compared to experimental data.

Analysis

General forms of the energy, momentum, and continuity equations served as the starting point for this model. These general equations are presented. Assumptions and simplifications required to obtain the one dimensional scalar equations in the axial direction which were solved are stated. The one dimensional scalar equations are also presented. In all cases a singly ionized, steady-state, quasi-neutral plasma was considered (*i.e.* $n_e=n_i$). Neglecting radiation, viscous disipation, and flow work the general form of the electron energy equation considered was[4]:

$$\nabla \cdot \left(\vec{U}_e n_e \frac{m_e \vec{U}_e^2}{2} + \vec{U}_e n_e \frac{5}{2} k T_e \right) = - \nabla \cdot q_e + \vec{J}_e \cdot \vec{E} - \sum_j \frac{2m_e}{m_j} \nu_{ej} n_e \frac{3}{2} k(T_e - T_j) - \varepsilon_i w \qquad 1a)$$

The convective flux of kinetic energy on the right hand side of the previous equation included the flux of azimuthal kinetic electron energy (i.e. $\vec{U}_e^2 = U_{ez}^2 + U_{e\theta}^2$). Therefore, neglecting heat conduction, the electron energy equation was written as:

$$\frac{3}{2} n_e m_e (U_e^2 + U_{e\theta}^2)\frac{dU_e}{dz} + \frac{1}{2} m_e U_e (U_e^2 + U_{e\theta}^2)\frac{dn_e}{dz} + \frac{5}{2} U_e n_e k \frac{dT_e}{dz} - n_e e U_e \frac{d\phi}{dz} =$$

$$-3\frac{m_e}{m_a} \nu_{ea} n_e k (T_e - T_a) - 3\frac{m_e}{m_i} \nu_{ei} n_e k (T_e - T_i) - (\varepsilon_i + \frac{5}{2} k T_e) w - n_e m_e U_e U_{e\theta} \frac{dU_{e\theta}}{dz} \qquad (1b)$$

This was the form of the electron energy equation which was solved. Similarly, in general form, neglecting the ion pressure gradient, electron-ion and atom-ion collisional momentum exchange, gravitational forces, shear stresses, and magnetization of ions, the ion momentum equation was given by:

$$n_e m_i \vec{U}_i \cdot \nabla \vec{U}_i = e n_i \vec{E} - m_i \vec{U}_i w \qquad (2a)$$

or in one dimension:

$$n_e e \frac{d\phi}{dz} + n_e m_i U_i \frac{dU_i}{dz} = - m_i U_i w \qquad (2b)$$

The previous assumptions were made on the basis that the dominate force on the ions is the electric field component of the Lorentz force. Identically, without simplification, the steady state ion continuity was:

$$\nabla \cdot (n_i \vec{U}_i) = w \qquad (3a)$$

or in one dimension:

$$n_e \frac{dU_i}{dz} + U_i \frac{dn_e}{dz} = w \qquad (3b)$$

The electron momentum equation was considered neglecting shear stresses and gravitational forces. In this case the general form of the electron momentum vector equation was[4]:

$$n_e m_e (\vec{U}_e \cdot \nabla \vec{U}_e) + \nabla P_e = -e n_e \vec{E} + \vec{J}_e \times \vec{B} - \sum_j n_e m_e \nu_{ej} (\vec{U}_e - \vec{U}_j) - m_e \vec{U}_e w \qquad (4a)$$

or in one dimension:

$$n_e k \frac{dT_e}{dz} + k T_e \frac{dn_e}{dz} + n_e m_e U_e \frac{dU_e}{dz} - n_e e \frac{d\phi}{dz} =$$

$$n_e e U_{e\theta} B_r - n_e m_e \nu_{ea} (U_e - U_a) - n_e m_e \nu_{ei} (U_e - U_i) - m_e U_e w \qquad (4b)$$

Again, although this equation is the axial component of the electron momentum equation, it includes the azimuthal electron velocity. This term, resulting from the $\vec{J}_e \times \vec{B}$ Lorentz term is thought to be critical for accurately modeling the axial motion of electrons. However, the radial magnetic field and azimuthal electron velocities are treated as input parameters to the model.

This differs from an alternate approach [2,3] utilized by previous investigators who neglect the Lorentz force due to the magnetic field as well as the convective term and the electron production term. For this case, the electron momentum equation became:

$$\nabla P_e = -e n_e \vec{E} + n_e m_e \nu_{ei} (\vec{U}_e - \vec{U}_i) \qquad (5)$$

Assuming the ion drift velocity is negligible with respect to the electron drift velocity, the electron mobility and a electron diffusion coefficient were defiened such that:

$$\vec{U}_e = -\mu_e \vec{E} - D_e \frac{\nabla P_e}{P_e} \qquad (6)$$

where,

$$\mu_e = \frac{e}{m_e \nu_{ei}} \quad \text{and} \quad D_e = \frac{k T_e}{m_e \nu_{ei}} \qquad (7,8)$$

For cases where there are strong magnetic fields, the classical diffusion coefficient has been shown to be insufficient to correctly describe electron motion. In this case, the empirical Bohm diffusion coefficient was used.

$$D_{Bohm} \approx \frac{kT_e}{16e\,B} \tag{9}$$

This approach relaxes the necessity of knowing the azimuthal electron velocity, decoupling the axial component of the electron momentum equation from the azimuthal component. However, the solution relies on an empirical diffusion coefficient that has not been shown to be applicable in this case.

The last differential equation used in this model to form a solution set was the atom momentum equation. The generalized form used neglected gravitational forces, shear stresses, atom pressure, electron-atom collisional momentum exchange, and the net rate of production of atom momentum due to ionization and recombination :

$$n_a m_a (\vec{U}_a \cdot \nabla \vec{U}_a) = - n_a m_a \nu_{ai} (\vec{U}_a - \vec{U}_i) \tag{10a}$$

or in one dimension:

$$n_a m_a U_a \frac{dU_a}{dz} = - n_a m_a \nu_{ai} (U_a - U_i) \tag{10b}$$

The term accounting for atom-ion mometum exchange, which was retained in equation 10, was neglected in the ion momentum equation because the amount of momentum transfered to the ions by collisions with atoms is negligible with respect to the acceleration of the ions by the electric field. Two remaining algebraic equations were used to form a closed set of equations: current continuity and global continuity.

$$n_e e U_i A - n_e e U_e A = J \tag{11}$$

$$n_a m_a U_a + n_e m_i U_i = \frac{\dot{m}}{A} \tag{12}$$

For this investigation A was considered constant throughout the computational domain, which does not accurately descide the expansion takes place downstream of the discharge chamber exit. Equations 1b, 2b, 3b, 4b, 10b, 11, and 12 form a set of seven coupled algebraic and differential equations with seven unknowns: U_e, U_i, U_a, T_e, n_e, n_a, ϕ. Magnetic field strength and azimuthal electron velocity appear as a product in the relevant equations, and as a result were treated as a single lumped parameter. The net rate of production of electrons and ions and the collisional momentum exchange frequencies were calculated in the following fashion. w, the net rate of electron/ion production is calculated based on the rate of ionization from electron impact and the rate of recombination due to collisions with the discharge chamber walls (based on a Bohm velocity).

$$w = n_e n_a k_i - n_e \left[\frac{kT_e}{2\pi m_i}\right]^{1/2} \tag{13}$$

Because the computational domain extends beyond the exit of the discharge chamber, the loss term is set to zero outside the discharge chamber. The rate of ionization, k_i is calculated based on the following integral:

$$k_i = \sqrt{\frac{2}{m_e}} \int_{Ei}^{\infty} \sqrt{E}\, f(E)\, Q(E) dE \tag{14}$$

where f(E) was assumed to be a Maxwellian electron energy distribution function, *i.e.*:

$$f(E) = \frac{2}{\sqrt{\pi}} \left(\frac{1}{kT_e}\right)^{3/2} E^{1/2} exp(-E/kT_e) \tag{15}$$

and Q(E), the collision cross section for ionization, was initially based on the empirical formulation presented by Drawin[5].

$$Q(E) = 2.66\pi a_0^2 \left(\frac{E_i^H}{E_i}\right)^{3/2} \frac{E/E_i - 1}{(E/E_i)^2} \ln(1.25E/E_i)\, dE \qquad (16)$$

Experimentally measured cross section were alternatively used[6,7]. The numerically integrated rate constants obtained using equation (14) are shown in Figure 2 based on the empirical collision cross sections and the experimental values. While the experimental cross sections seem significantly different, the calculated rates show a much smaller difference. The effect of using these different rates will be discussed along with the results.

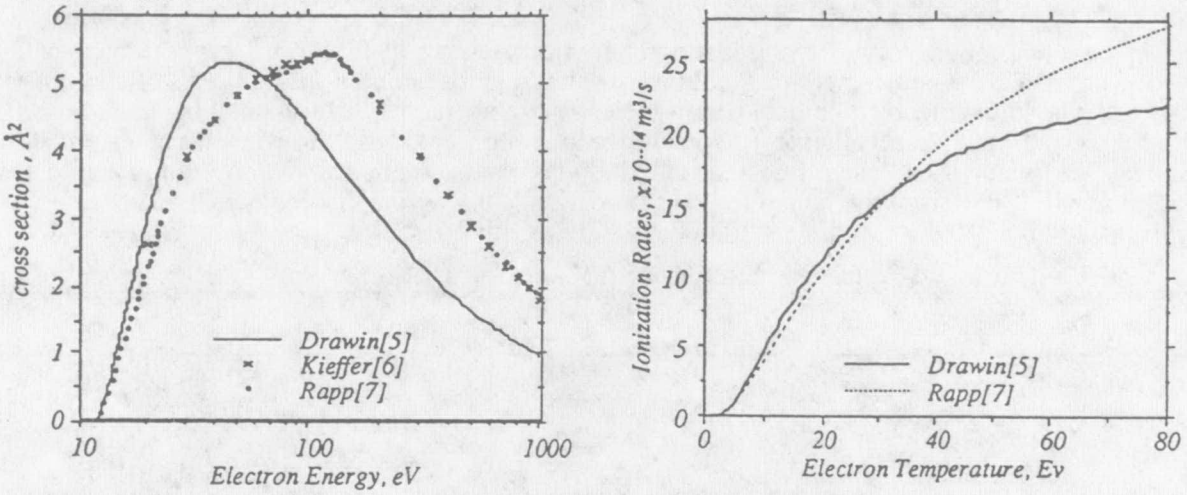

Figure 2: Total ionization cross section for ionization of atomic xenon by electron bombardment and calculated rates of ionization assuming an Maxwellian electron energy distribution function.

The electron-ion momentum transfer collision frequency was taken from Mitchner and Kruger[8]. This expression was:

$$\nu_{ei} = n_i \frac{4\sqrt{2\pi}}{3} \left(\frac{m_e}{kT_e}\right)^{3/2} \left(\frac{e^2}{4\pi\varepsilon_o m_e}\right)^2 \ln\left(1.24 \times 10^7 \left(\frac{T_e^2}{n_e}\right)^{1/2}\right) \qquad (17)$$

For electron-atom and atom-ion momentum transfer collisions the geometric cross section was used.

$$\nu_{ea} = n_a \langle\sigma\rangle \left(\frac{8kT_e}{\pi m_e}\right)^{1/2} \quad \text{and} \quad \nu_{ai} = n_i \langle\sigma\rangle U_i \qquad (18,19)$$

In all cases charge exchange collisions within the discharge were neglected. The previously mentioned closed set of equations was solved in the following fashion. $\frac{dU_e}{dz}$ was eliminated from eqns. 1-4 using eqn. 11. These four equations were recast in the following matrix form $A\vec{x} = \vec{b}$

$$\begin{bmatrix} \frac{5}{2}U_e n_e k & -n_e e U_e & 0 & -m_e U_e(U_e^2 - U_{e\theta}^2) \\ 0 & n_e e & n_e m_i U_i & 0 \\ 0 & 0 & 1 & U_i/n_e \\ n_e k & -n_e e & 0 & kT_e + m_e U_e U_i - m_e U_e^2 \end{bmatrix} \begin{bmatrix} \frac{dT_e}{dz} \\ \frac{d\phi}{dz} \\ \frac{dU_i}{dz} \\ \frac{dn_e}{dz} \end{bmatrix} = \begin{bmatrix} b_1 \\ b_2 \\ b_3 \\ b_4 \end{bmatrix}$$

where $\vec{b}$ is:

$$\begin{bmatrix} b_1 \\ b_2 \\ b_3 \\ b_4 \end{bmatrix} = \begin{bmatrix} -3\frac{m_e}{m_a}\nu_{ea}n_e k(T_e-T_a) - 3\frac{m_e}{m_i}\nu_{ei}n_e k(T_e-T_i) - (\varepsilon_i + \frac{5}{2}kT_e + \frac{3}{2}m_e(U_e^2 + U_{e\theta}^2))\,w - n_e m_e U_e U_{e\theta}\frac{dU_{e\theta}}{dz} \\ -m_i U_i w \\ w/n_e \\ n_e e U_{e\theta} B_r - n_e m_e \nu_{ea}(U_e-U_a) - n_e m_e \nu_{ei}(U_e-U_i) - m_e U_e w \end{bmatrix}$$

This system was then solved by recasting the matrix equation into a tridiagonal form and back substitutiing. This type of marching solution required initial conditions for each of the differential equation. The initial electron number density, electron temperature, electric potential and, atom and ion velocity were given. The values used for the initial conditions and the assumed values are shown in Table I. Due to numerical instabilities, the solution was restricted to positive temperature gradients in the initial portion of the discharge chamber even though negative gradients may exist. The use of a more sophisticated higher order solution technique might relax this constraint.

Table I: Initial Conditions and Assumed Values For the Simplified Numerical Model

Initial Conditions	Assumed Values	
$n_e = 1\text{x}10^{16}$ m^{-3}	$T_i = 1000$K	$\dot{m} = 4.5$ mg/s
$T_e = 5$eV	$T_a = 1000$K	$A = 0.0054$ m^2
$U_i = 500$ m/s	$U_a = 500$ m/s	$B_{rmax} = 130$ Gauss
$\phi = 0$ Volts	$J = 4.5$ Amperes	$U_{e\theta max} = 1\text{x}10^{16}$ m/s

Results and Discussion

Analytical solutions were generated for a 3.6 cm long computational domain using the experimental collision cross sections. The length of the discharge chamber was 2 cm. These dimensions correspond to the geometry of the SPT-100. The radial magnetic field was given the Gaussian axial distribution shown in Figures 1 and 3. The azimuthal electron velocity was also assumed to have this functional dependance. This was deemed appropriate because the radial magnetic field is the primary mechanism for imparting azimuthal electron motion. The distribution was an analytic estimate of the actual magnetic field distribution. The peak value of the azimuthal electron velocity was calculated based on measured values of electron number density and azimuthal electron current[9,10]. The resulting potential distribution with the cathode potential set to zero, normalized assumed magnetic field distribution, electron number density and electron temperature are shown in Figure 3.

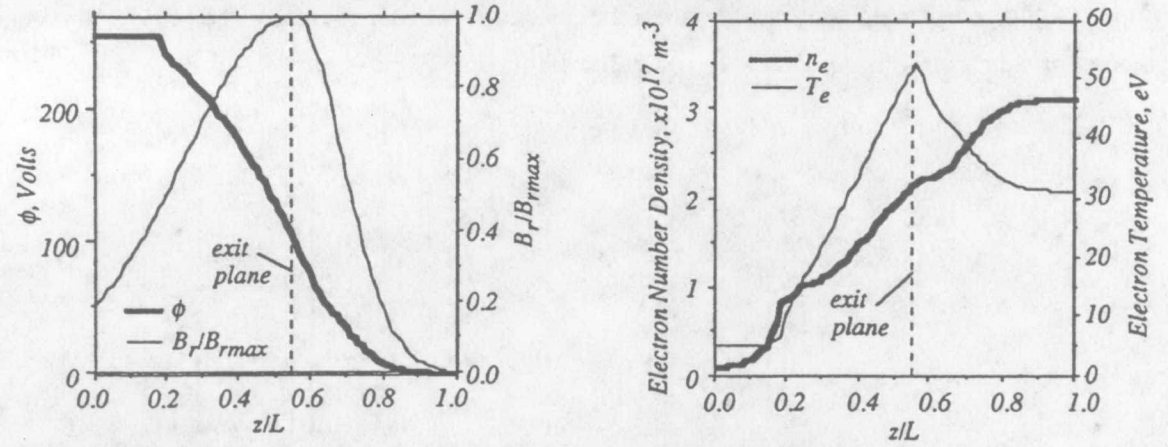

Figure 3: Spatial Distribution of the Calculated Potential, Electron Number Density and Electron Temperature and the input Radial Magnetic Field Distribution.

The potential dropped slowly until the magnetic field strength was sufficiently intense to significantly imped axial electron motion. In the region from $z/L = 0.2$ to 0.8 the potential dropped rapidly. Closer to the cathode plane the potential asymptoted to its final value. The total potential drop was approximately 250 Volts which is comparable with the 300 Volt discharge voltage considered nominal for SPT-100 operation. The electrode phenomena which were not included in this model may have contributed to this discrepancy. The maximum calculated axial ion velocities were 12000 m/s, which corresponds to a specific impulse of 1220 seconds, slightly below the nominal measured specific impulse of 1500 seconds.

The electron/ion number density increased gradually from the initial value of 10^{16} m^{-3} throughout the discharge until $z/L = 0.8$, beyond which it was nearly constant. The initial value corresponded to a ionization fraction of 0.001 or 0.1% at the anode. This value was chosen arbitrarily and a sensitivity analysis on this initial condition was not performed during this preliminary study. The peak value was approximately $3x10^{17}$ m^{-3}. In terms of the percent of ionization, the plasma was essentially fully ionized by the exit, however, the ionization fraction didn't reach 0.90 until z/L =0.9. This indicated that ionization is occurring throughout the entire region of the discharge. The creation of the majority of electron/ion pairs at axial locations ranging from an z/L of 0.2 to 0.8 correspond to a location in the potential distribution where the majority of the potential drop occurred. This suggests that Joule heating of the electrons in the regions of high electric field strength, caused by significant radial magnetic field strengths, gave rise to effective ionization of neutral xenon in this region of the discharge which were subsequently accelerated away.

The electron temperature was relatively constant in the initial portion of the discharge chamber where it was forced to have a positive gradient. Peak values of approximately 51 eV were obtained between the exit of the discharge chamber and the cathode plane. The calculated ionization rates had a measurable effect on this maximum value. When the rates generated using Drawin's empirical ionization cross sections were used a maximum electron temperature of 60 eV was calculated. Additionally, the ionization fraction at the exit dropped to 0.95 and the potential drop increased by 40 Volts to 290 Volts. Because of the excellent agreement between the various measurements of ionization cross sections these values were thought to be accurate. Consequently, the empirical values of ionization cross sections presented by Drawin, which had initially been adapted for convenience, were not used.

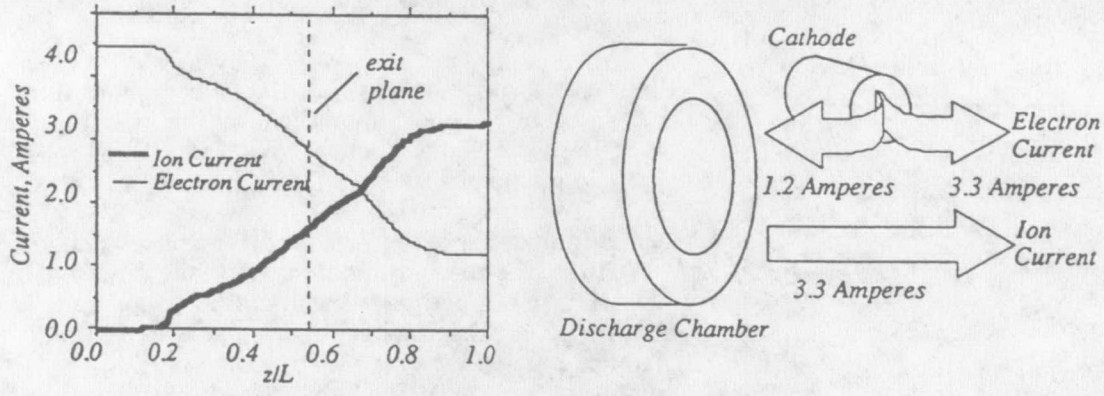

Figure 4: Calculated Electron and Ion Current as a Function of Axial Position. Electron and Ion Currents at the Cathode Plane Showing Neutralization.

Due to the reduced axial electron plasma conductivity the electrons were not the only significant current carriers. As can be seen in Figure 4, the ions also carried a significant portion of the current. Near the anode the electrons essentially carried all the current. The amount of ion current increases and equals the electron current at an z/L of 0.7. In the remainder of the discharge the ions carried the majority of the current. However, the maximum ion current was restricted by the assumption of only singly ionized ions. For the supplied mass flow rate of 4.5 mg/s this corresponds to a maximum ion current of 3.3 Amperes. What this implied was that the cathode supplied 1.2 Amperes to the discharge and the remaining 3.3 Amperes needed to neutralize the exiting ion beam as depicted in Figure 4. There is, however, the possibility during actual operation of ion beam currents in excess of the discharge current

due to the presence of multiply charged ions. This has previously been observed[11]. In this instance, the exiting ion beam would be neutralized by the electron current from the cathode, equal to the discharge current, and additional electrons from the discharge. Before these two sources of electrons, (*i.e.* from the discharge and from the cathode), had experienced sufficient thermalizing collisions a non-equilibrium electron energy distribution function would exist consisting of the sum of two different equilibrium electron energy distribution functions. This is offered as a potential explanation of the non-equilibrium distribution experimentally observed [12,13]. If the electron energy distribution function was not Maxwellian within the discharge chamber, the rates used in the simplified numerical model developed during this investigation were invalid and these results do not apply.

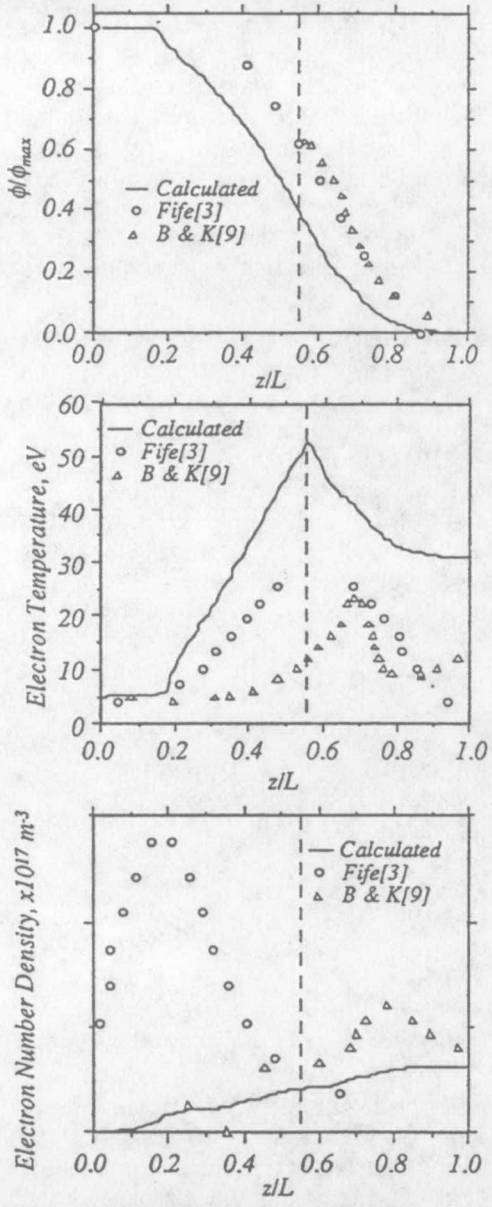

Figure 5: Comparison of normalized Potential, Electron Temperature, and Electron Number Density with Fife[3] and Bishaev and Kim[9]

Calculated solutions were compared to the those of Fife[3] and the measurements taken by Bishaev and Kim[9]. These comparisons are shown in Figure 5. In each of these investigations the discharge chamber was approximately 5 cm long. In the SPT-100 the discharge chamber was approximately 2 cm long, therefore direct comparisons with these previous investigations required some form of normalization. The length of the discharge chamber was chosen. This distance was used rather than the anode to cathode distance since cathode position was not considered as critical. Furthermore, because the total potential drop was 200 Volts in the case of Fife and Bishaev and Kim the values were normalized by the maximum potential value. Additionally, their data were presented in two dimensions. Comparisons were made with their annular centerline values. The normalized potential distributions were similar with the majority of the potential drop taking place in a region near the exit of the discharge chamber and very little potential drop in the first half of the discharge chamber. Slight differences in the distribution may be attributed to the normalization scheme or differences in the thrusters being considered.

The calculated values of electron temperature were considerably higher than those calculated by Fife and measured by Bishaev and Kim. The overall magnitudes were considerably higher. Both these results and the calculated results of Fife show a peak in electron temperature at or near the exit of the discharge chamber ($z/L = 0.56$). The measurements of Bishaev and Kim showed an electron temperature distributions with a peak midway between the discharge chamber exit and the cathode plane. Higher calculated exit electron maybe the result of not including an expansion downstream of the constant area discharge chamber in the one-dimensional model presented here.

The electron number densities are also compared. The calculated values and measurements between Bishaev and Kim show similar characteristics: peak values of approximately 3 to 5×10^{17} m^{-3} between the discharge chamber exit and the cathode. The calculated values of Fife showed a substantially higher peak value occurring upstream of the midpoint of the discharge chamber.

Concluding Remarks

A simplified numerical model of the plasma discharge within the SPT-100 stationary plasma thruster was presented. Seven coupled algebraic and differential equations, which included ion continuity, global continuity, current continuity, ion momentum, electron momentum and electron energy were shown to form a minimum subset of equations which retained all the essential physics, providing azimuthal electron velocities were included as an input parameter. Based on a consideration of the SPT-100 geometry with a 4.5 mg/s anode flow, 4.5 Amperes of discharge current, and a peak radial magnetic field strength of 130 Gauss, a quasi-one dimensional description used provided a solution set. This solution indicated peak plasma densities of approximately 3×10^{17} m^{-3} between the discharge chamber exit and the cathode. Peak electron temperatures of 51 eV were calculated. This result was sensitive to the collision cross sections for ionization of xenon by electron impact. Ionization fractions of 1 were calculated near the cathode plane. The calculated potential distribution showed the majority of drop in the region of peak radial magnetic field strength, with a magnitude of 250 Volts. Calculated plasma densities and potential distribution compare favorably with previous measurements. Calculated electron temperatures are substantially higher than previously reported.

References

1 Melikov, I, "Equilibrium Flow in a Hall Current Plasma Accelerator," *Sov. Phys. Tech Phys.*, Vol. 19, No. 3, Sept. 1974, pp.343-346.

2 Lentz, C.A., "Transient One Dimensional Numerical Simulation of Hall Thrusters," AIAA-93-2491, June 1993.

3 Fife, M.,J., "Two-Dimensional Hybrid Particle-In-Cell Modelling of Hall Thrusters," Thesis Master of Science, Department of Aeronautics and Astronautics, Massachusetts Institute of Technology, May 1995.

4 Bittencourt, J.A., *Fundamentals of Plasma Physics*, Permagon Press, Oxford, 1986, pp. 205-211.

5 Drawin, H., "Collision and Transport Cross Sections," EUR-CEA-FC-383, 1966.

6 Kieffer, L.J., "Low-Energy Electron-Collision Cross Section Data Part I: Ionization Dissociation, Vibrational Excitation," *Atomic Data*, Vol.1, 1970, p.19.

7 Rapp, D. and Englander-Golden, P., "Total Cross Sections for Ionization and Attachment in Gases by Electron Impact. I. Positive Ionization," *Chem. Phys.*, vol 43, No. 5, Sept. 1965, pp.1464-1479.

8 Mitchner, M. and Kruger C.H., *Partially Ionized Gases*, John Wiley and Sons, New York, 1973.

9 Bishaev, A.M. and Kim,V., "Local Plasma Parameters in a Hall-Current Accelerator with an Extended Acceleration Zone," *Sov. Phys. Tech Phys.*, Vol. 23, No. 9, Sept. 1978, pp.1055-1057.

10 Bugrova, A.I., Morozov,A.I., and Kharchevnikov, V.K., "Probe Measurements of Drift Current in a Hall Accelerator," *Sov. Phys. Tech Phys.*, Vol. 30, No. 6, June 1985, pp.610-612.

11 Manzella, D.H. and Sankovic, J.M., "Hall Thruster Ion Beam Characterization," AIAA-95-2927, July 1995.

12 Bugrova, A.I., Versotskii, V.S., Kalikhman, L.E., and Morozov, A.I., "Experimental Determination of the Electron Distribution Function in a Plasma Stream," *Teplofizika Vysokikh Temperatur*, Vol. 16, No. 5, Sept. 1978, pp. 937-942.

13 Bugrova, A.I., Volkova, L.M., Ermolenko, V.A., Kral'kina, E.A., Devyatov, A.M. and Kharchevnikov, V.K.., "Dynamics of the Electron Energy Distribution Function in a Plasma Accelerator withExtended Acceleration Zone" *Teplofizika Vysokikh Temperatur*, Vol. 19, No. 6, Nov. 1981, pp. 937-942.